G&G Gem News International

Contributing Editors
Emmanuel Fritsch, *University of Nantes, CNRS, Team 6502, Institut des Matériaux Jean Rouxel (IMN), Nantes, France* (fritsch@cnrs-imn.fr)
Gagan Choudhary, *Gem Testing Laboratory, Jaipur, India* (gagan@gjepcindia.com)
Christopher M. Breeding, *GIA, Carlsbad* (christopher.breeding@gia.edu)

COLORED STONES AND ORGANIC MATERIALS

Discovery of color-change chrome grossular garnets from Ethiopia. Ethiopia has become a significant producer of opal, sapphire, and emerald in recent years. In addition, reports of gem-quality green garnets have started to emerge (B. Williams et al., "Tsavorite reportedly from Ethiopia," *Journal of Gemmology*, Vol. 35, No. 8, 2017, pp. 702–704).

Todd Wacks (Tucson Todd's Gems, Tucson, Arizona, and Vista, California) recently submitted three rough and one faceted garnet (figure 1, stones 1, 2, 3, and 4) to GIA in Carlsbad for scientific examination. He purchased the garnets from Inna Gem, which reported that the garnet mine is located near the town of Wbi and the new Dubuluk emerald deposit (Spring 2017 GNI, pp. 114–116). The stones showed obvious color change from yellow-green under daylight-equivalent lighting to orange-brown under incandescent illumination. This is similar to the color-change behavior reported for some color-change garnets from Sri Lanka (Spring 2017 GNI, pp. 137–138).

Standard gemological testing revealed a refractive index (RI) of 1.740 on the faceted stone. Hydrostatic specific gravity (SG) of all garnets in this study ranged from 3.62 to 3.68. Fluorescence was inert to long-wave and short-wave UV light. Rotating the stones 360° between a pair of crossed polarizing filters revealed an anomalous double refraction. Using a handheld spectroscope, faint absorption bands at 480–490 and 570–590 nm were observed. Microscopic examination showed fingerprints composed of two-phase inclusions, iron-stained and cloudy fractures, long thin etch channels, unidentified transparent crystals, and zoned greenish brownish yellow areas. These properties are consistent with grossular (grossular-andradite) garnets (I. Adamo et al., "Tsavorite and other grossulars from Itrafo, Madagascar," Fall 2012 *G&G*, pp. 178–187; M.L. Johnson et al., "Gem-quality grossular-andradite: A new garnet from Mali," Fall 1995 *G&G*, pp. 152–166.).

Laser ablation–inductively coupled plasma–mass spectrometry (LA-ICP-MS) analyses were performed to obtain the chemical composition of these garnets using a Thermo Fisher iCAP Qc ICP-MS coupled with an ESL NWR213 nm laser ablation unit. USGS glass standards GSD-1G and GSE-1G and NIST glass standard 610 were used as external standards. ^{29}Si was used as an internal standard. The analyses were performed in the same region where spectroscopic data was collected for stones 3, 4 (Ethiopian garnets), 5 (non-Ethiopian tsavorite), and 6 (non-Ethiopian demantoid) (see www.gia.edu/gems-gemology/summer-2018-gemnews-discovery-of-color-change-chrome-grossular-garnets-from-ethiopia). The Ethiopian garnets are predominantly composed of 87.24–91.60% grossular, 6.03–8.19% andradite, 1.04–2.80% spessartine, 1.29–0.55% uvarovite, 0.71–0.82% pyrope, and 0.03–0.05% goldmanite (again, see stones 1–4 at the link provided above). The dominant chromophore is Cr^{3+} at about 0.19–0.43 wt.%, with an almost negligible contribution from V^{3+}. This contrasts significantly with most tsavorite grossular garnets, whose color is dominantly derived from V^{3+} with a lesser contribution from Cr^{3+} (Adamo et al., 2012).

UV-Vis-NIR spectra (figure 2) were collected and corrected for reflection loss. These spectra were then used to quantitatively calculate the color of the garnets at a wide range of path lengths and under different lighting conditions. In addition to two of the Ethiopian grossular garnets, UV-Vis spectra were also collected on the non-Ethiopian tsavorite (stone 5) and the non-Ethiopian demantoid (stone 6) for comparison. The chemistry of stones 5 and 6 is also reported online; see the link above. The calculated color panels of stones 3–6 under daylight-equivalent lighting (CIE D65 illumination) and incandescent light (CIE A illumination) are shown in figure 3, which shows the pos-

Editors' note: Interested contributors should send information and illustrations to Stuart Overlin at soverlin@gia.edu or GIA, The Robert Mouawad Campus, 5345 Armada Drive, Carlsbad, CA 92008.

Gems & Gemology, Vol. 54, No. 2, pp. 233–254.

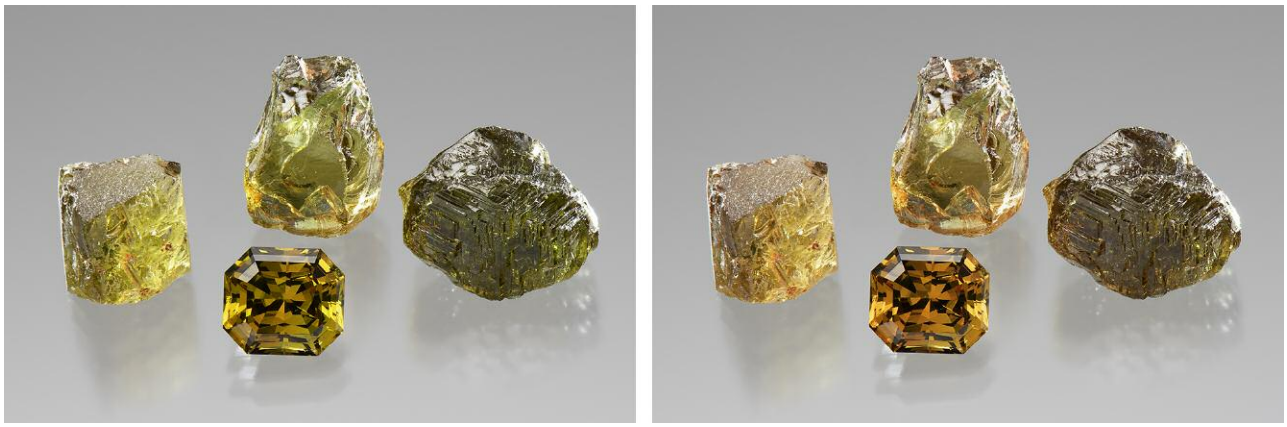

Figure 1. Left: Three rough garnets (left to right, stones 2, 3, and 4) and one faceted garnet photographed in an LED light source with 6000K color temperature (a daylight-equivalent light simulator). Right: The same stones photographed in an LED light source with 3100K color temperature (an incandescent light simulator). The 2.705 ct faceted stone measures 8.08 × 7.18 × 5.49 mm. Photos by Kevin Schumacher.

sible colors these four garnets would exhibit with different path lengths (defined by stone thickness) and the approximate corresponding carat weight of a well-proportioned round brilliant (for details of this calculation, see Z. Sun et al., "Vanadium- and chromium -bearing pink pyrope garnet: Characterization and quantitative colorimetric analysis," Winter 2015 *G&G*, pp. 348–369). Ethiopian grossular stone 4 showed a stronger color change and a higher chromium component than Ethiopian grossular stone 3. Stone 6 showed a more yellowish green than stone 5 due to the demantoid's higher Fe component, which absorbs more blue light than in tsavorite (again, see figure 2).

One way to judge the quality of a color-change stone is to plot the color panel pair in the CIE 1976 color circle. Good color-change pairings show a large hue angle difference, a small chroma difference, and large chroma values (Z. Sun et al., "How to facet gem-quality chrysoberyl: Clues from the

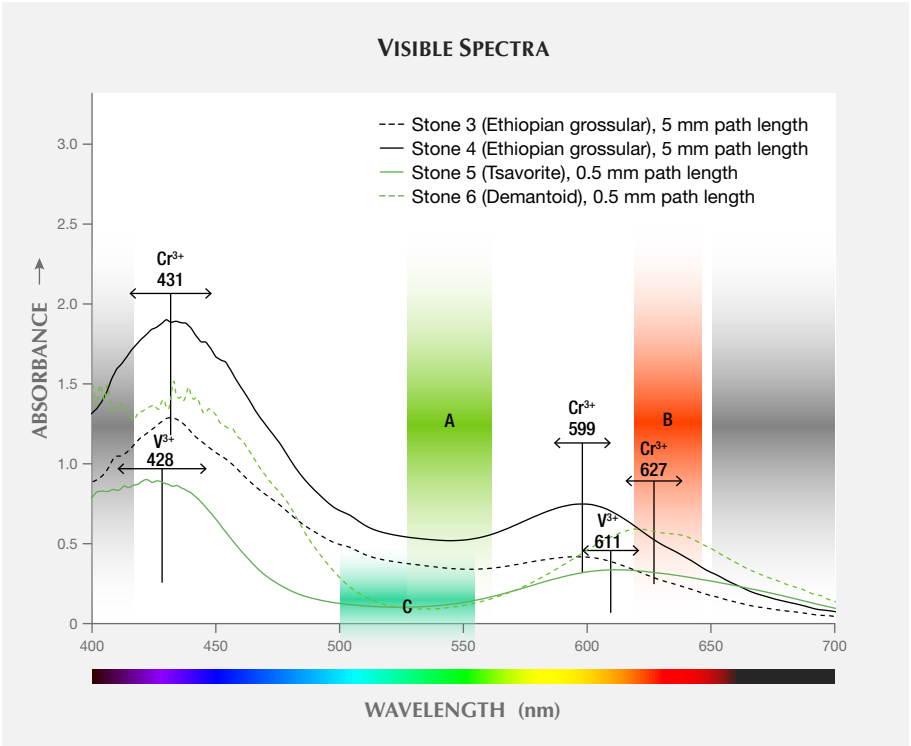

Figure 2. The calculated visible absorption spectra (corrected for reflection loss) of garnets 3, 4, 5, and 6 with various path lengths. Transmission window A is centered at 545 nm. Transmission window B is between 620 and 650 nm; transmission window C is centered at 520 nm. In Ethiopian grossular stones 3 and 4, the absorption bands at 431 and 599 nm are caused by Cr^{3+}. In stone 5 (non-Ethiopian tsavorite) the absorption bands at 428 and 611 nm are caused by V^{3+}. In stone 6 (non-Ethiopian demantoid) the absorption bands at 431 and 627 nm are caused by Cr^{3+} (Adamo et al., 2009). The human eye is not color sensitive above 650 nm or below 420 nm wavelength (gray color zoning in the graph). The transmission in these ranges cannot contribute to the color seen. Please note that the y-axis units are in true absorbance and not absorbance coefficients.

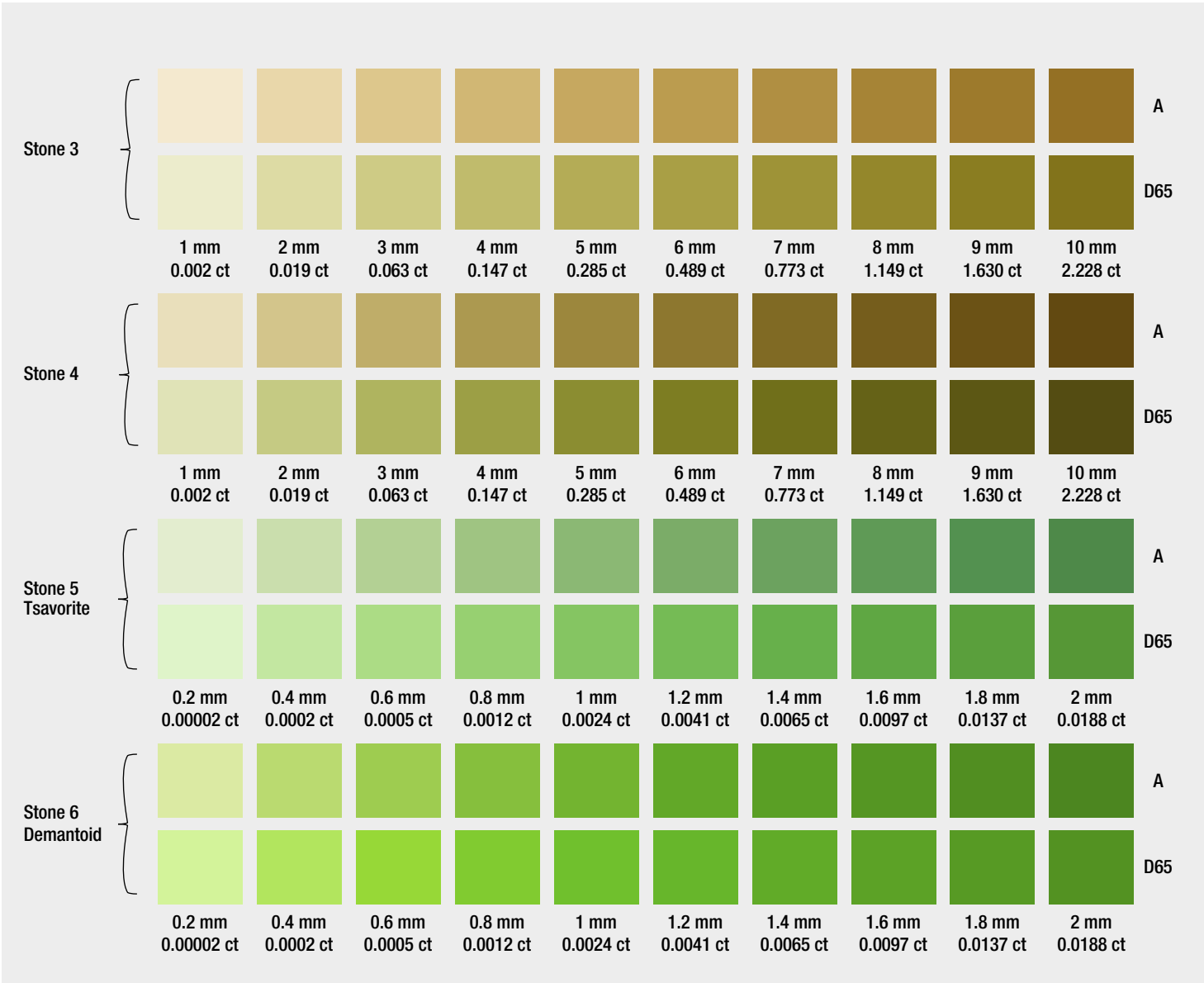

Figure 3. The color panels of four garnets (stones 3, 4, 5, and 6) under CIE A (incandescent) and CIE D65 (daylight-equivalent) illumination are quantitatively reproduced. The garnets' colors are shown at different light path lengths (defined by stone thickness). For each sample, the top and bottom rows represent the color under incandescent light (A) and daylight-equivalent light (D65), respectively. For calculation methods, please see Sun et al. (2017).

relationship between color and pleochroism, with spectroscopic analysis and colorimetric parameters," *American Mineralogist*, Vol. 102, No. 8, 2017, pp. 1747–1758). The color coordinates of the four stones in daylight-equivalent (D65) and incandescent (A) illumination were plotted in the CIE 1976 color circle (see the link above). Ethiopian grossular stone 4 had the largest hue angle difference among the four stones and a relatively small chroma difference. The non-Ethiopian tsavorite and demantoid both had a very small hue angle difference that was close to zero but with large chroma difference.

One interesting observation is that the Cr^{3+} absorption band shifted significantly from 627 in demantoid (stone 6) to 599 in the Ethiopian grossulars (stones 3 and 4; all stone samples contained little V). This shift opens a transmission window B in the red region shown in figure 2. To our knowledge, color-change behavior has not been reported in tsavorite or demantoid. This is because the absorption bands of V^{3+} at the 610 region in tsavorites (green grossular) or of Cr^{3+} at the 627 nm region are dominated by Cr^{3+} in demantoids and prevent the transmission of red light in these stones. In other words, there is no transmission win-

TABLE 1. Vanadium and chromium concentration of grossular garnets, obtained by LA-ICP-MS.

Ethiopian grossular from this study	
Oxide (wt.%)	
V_2O_3	0.01–0.02
Cr_2O_3	0.19–0.43

dow in the red for tsavorite or demantoid. However, these Ethiopian grossulars have little V^{3+}, and the Cr^{3+} absorption is shifted away from the red region, which allows for significant transmission of red light through these stones. This creates a transmission window that produces significantly different color for the Ethiopian grossular in incandescent illumination versus daylight. To the authors' knowledge this was the first group of color-change gem-quality chrome grossular garnet reported.

Ziyin Sun, Aaron C. Palke, Nathan D. Renfro, Heidi Breitzmann, Dylan Hand, and Jonathan Muyal
GIA, Carlsbad

Green-blue Maxixe-type beryl. Recently, a transparent greenish blue pear-shaped mixed-cut sample (figure 4) was submitted for identification to the Gem Testing Laboratory in Jaipur. The 54.21 ct specimen (40.00 × 20.14 × 12.63 mm) was relatively clean to the unaided eye. Its RI of 1.582–1.590, birefringence of 0.008 with a uniaxial negative optic sign, and hydrostatic SG of 2.71 suggested a beryl, which was later confirmed with Fourier-transform infrared (FTIR) and Raman spectroscopy. The specimen's natural origin was established by zones of fine growth tubes, planes of dendritic platelets (usually ilmenite, although not identified here) oriented along the basal plane, and birefringent crystals.

Identification of the stone as beryl was straightforward, but its unusual color and striking dichroism invited further study. It displayed deep blue and yellow as the two principal colors (figure 5); the deep saturated blue resembled the color

Figure 4. This 54.21 ct green-blue specimen was identified as Maxixe-type beryl. Photo by Gagan Choudhary.

of top-quality sapphires. Such strong dichroism was reminiscent of Maxixe-type beryls, although their dichroic colors are usually deep blue and colorless. Careful examination of the specimen showed a deep saturated blue o-ray and a yellow e-ray. Maxixe-type beryls are known to display deep blue color absorption along the o-ray direction (R. Webster, *Gems*, 5th ed., Butterworth-Heinemann, London, 1994, pp. 124–127) and colorless along the e-ray direction. An opposite pattern of deep blue (e-ray) and pale greenish blue (o-ray) absorptions was reported previously in an aquamarine by this author (Fall 2014 GNI, pp. 244–245).

Further analysis with UV-Vis-NIR spectroscopy confirmed the cause of color. Polarized spectra (figure 6) revealed a series of bands between 500 and 700 nm along the o-ray direction, but only a broad absorption feature at ~690 nm along the e-ray; these features are typically associated with the radiation-induced color centers observed in Maxixe-type beryl (see I. Adamo et al., "Aquamarine, Maxixe-type beryl, and hydrothermal syn-

Figure 5. The Maxixe-type beryl in figure 4 displayed an intense dichroism, with a deep saturated blue o-ray (left) and a yellow e-ray (right). A combination of these blue and yellow components resulted in a greenish face-up appearance. Photos by Gagan Choudhary.

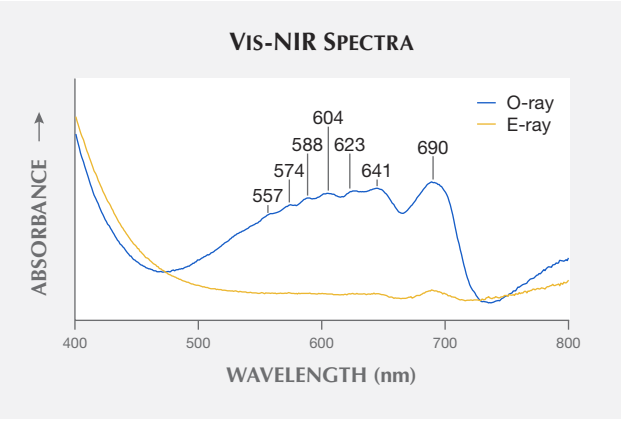

Figure 6. Polarized Vis-NIR spectra of the green-blue Maxixe-type beryl displayed a series of bands between 500 and 700 nm (o-ray) that are associated with radiation-induced color centers.

Figure 7. Left to right: 16.73 ct, 14.50 ct, 17.03 ct, and 27.75 ct trapiche-like amethysts. The four cabochons were cut with the base perpendicular to the c-axis (optic axis). Photo by Diego Sanchez.

thetic blue beryl: Analysis and identification," Fall 2008 *G&G*, pp. 214–226).

Gemological properties along with absorption spectra and the pleochroic color directions were sufficient to establish the identity of this submitted specimen as Maxixe-type beryl. This was the first time we had encountered a green-blue Maxixe-type beryl, although there exists a previous report of such a beryl (see K. Nassau et al., "The deep blue Maxixe-type color center in beryl," *American Mineralogist*, Vol. 61, 1976, pp. 100–107). On the basis of pleochroic colors, it can be deduced that the greenish face-up appearance of this specimen was due to the overlap of blue and yellow color components. The supplier of the specimen informed us that the specimen is reportedly from Mozambique.

Gagan Choudhary (gagan@gjepcindia.com)
Gem Testing Laboratory, Jaipur, India

Trapiche-like amethyst from Brazil. Minerals such as corundum, beryl, tourmaline, and quartz, which belong to either the trigonal or the hexagonal crystal system, can show a trapiche-like texture with a hexagonal core and six extended arms when viewed down the c-axis. Four trapiche-like amethyst cabochons (figure 7) were submitted to GIA's Carlsbad laboratory by L. Allen Brown (All That Glitters, Methuen, Massachusetts) for scientific examination. Each was characterized by a hexagonal black core and six brownish arms with pale purple color zoning in between. Magnification revealed that the black core was composed of dense metallic dendritic inclusions (figure 8, left). The brown color of the arms was caused by numerous tufts of tiny inclusions (figure 8, right), some of which resembled either brushes or bullets.

Raman spectra were collected with a Renishaw inVia Raman microscope system. The confocal capabilities of the

Figure 8. Left: Metallic dendritic inclusions compose the hexagonal black core in the amethysts; field of view 19.27 mm. Right: Brownish and yellowish brush-like and bullet-like fibrous inclusions in the trapiche-like arms; field of view 2.34 mm. Photomicrographs by Jonathan Muyal.

Figure 9. A 12-rayed black star sapphire, weighing 3.6 ct, with one set of golden rays and another set of silver rays producing two different-colored stars. Photo by Simon Bruce-Lockhart.

system allowed inclusions beneath the surface to be analyzed. The black core was identified as an FeS_2 (iron sulfide) mineral, likely pyrite. The brownish tiny inclusions in arms could not be identified but were likely goethite (E.J. Gübelin and J.I. Koivula, *Photoatlas of Inclusions in Gemstones*, Vol. 2, Opinio Verlag, Basel, Switzerland, p. 558) based on appearance and occurrence in quartz matrix.

The texture of trapiche-like amethysts is often caused only by the distribution of color-inducing elements (K. Schmetzer and B. Williams, "Gem-quality amethyst from Rwanda: Optical and microscopic properties," *Journal of Gemmology*, Vol. 36, No. 1, 2018, pp. 26–36). The fact that the texture was caused by two sets of distinctly colored inclusions makes these four gemstones unique.

Ziyin Sun, Jonathan Muyal, and Dylan Hand

Twelve-rayed star sapphire from Thailand. The Thai city of Chanthaburi is a well-known international trading hub for colored gemstones but was once an important corundum mining center. In recent decades, mining activity in the area has decreased, but there are still several smaller-scale operations active. The 3.6 ct 12-rayed black star sapphire shown in figure 9 was mined in 2017 in Bang Kha Cha (or Bang Kaja), a mining locality near Chanthaburi.

Thailand's gemstone deposits typically produce blue, green, and yellow sapphires (and combinations of these colors). The deposits in eastern Thailand also produce a peculiar sapphire variety: black star sapphire. This variety is found in other basalt-related deposits like Australia, but they rarely match the size, quality, and abundance that the Thai stones are famous for.

The black color is due to a very high concentration of Fe-rich particles, identified as hematite and ilmenite. This high density of particles completely masks the bodycolor of the stone. When strongly illuminated from the back, glimpses of the bluish green bodycolor in this gem can be seen. If the platy, Fe-rich particles are oriented in the correct way, they result in a six-rayed star pattern. This star is often yellowish golden in color.

Another common inclusion in corundum is rutile needles. When they are abundant and correctly oriented in the crystal, this might also result in a six-rayed pattern, often with a whitish silvery color. In some cases, both of these patterns overlap, creating a 12-rayed star with one set of golden-yellow rays and one set of silver-white rays. The stone in figure 9 is an excellent example of this phenomenon, displaying well-centered, sharp asterism with two different-colored stars.

Wim Vertriest
GIA, Bangkok

Simon Bruce-Lockhart
Chanthaburi, Thailand

Update on trace-element chemical characteristics of golden sheen sapphire. GIA's Tokyo laboratory recently examined 23 sapphires displaying a "golden sheen" effect, reportedly from Kenya (e.g., T.N. Bui et al., "From exsolution to 'gold sheen': A new variety of corundum," *Journal of Gemmology*, Vol. 34, No. 8, 2015, pp. 678–691). Bui et al. (2015) were the first to describe gemological characteristics of golden sheen sapphires from Kenya; updated characteristics of inclusions, UV-Vis-NIR spectra, and chemistry of golden sheen material was published the following year (N. Narudeesombat et al., "Golden sheen and non-sheen sapphires from Kenya," The Gem and Jewelry Institute of Thailand, July-August 2016, pp. 282–288; Winter 2016 Lab Notes, pp. 413–414). Here we update the gemological and chemical characteristics of the recently examined material, and compare the information with various sapphire sources including other golden sheen sapphire data previously documented.

We examined 15 cabochons, three faceted, and five rough stones (figure 10). The samples were semi-transparent to opaque, with a blue and yellow bodycolor and weight range of 1.75 to 34.00 ct. The cabochons displayed a "golden sheen" effect and/or golden six-ray asterism. For the polished samples, standard gemological testing revealed RI values of 1.760 to 1.770 and hydrostatic SG values of 3.98–4.01, except for one densely included stone with an SG of 4.04 (see Lab Notes this issue, pp. 212–213). These SG values suggested that they were all corundum. The rough stones showed SG values of 3.82–4.01 and the Raman signatures of corundum.

The inclusions were similar to those in other golden sheen sapphires described by Bui et al. (2015) and Narudeesombat et al. (2016). Characteristics included dense clouds composed of brownish needles and platelets displaying a golden sheen effect. Raman analysis identified the needles as ilmenite and hematite, although their Raman signals

Figure 10. Eighteen of the 23 golden sheen sapphires examined for their trace-element chemical characteristics. The largest stone weighs 34 ct. Photo by Shunsuke Nagai.

were weak because of their thinness. Some showed six-ray asterism caused by reflection from dense clouds of oriented needles. Inclusion-free zones like the center stone and rough stones in figure 1 contained mineral crystals and healed fissures with negative crystals (see Lab Notes, pp. 212–213). Various euhedral to subhedral mineral inclusions (figure 11) were confirmed as hematite, diaspore, and zircon. Hematite was found as needles and euhedral crystals; these euhedral hematite crystals coexisted with goethite (figure 11B). Some carbonate minerals such as siderite ($FeCO_3$) and dawsonite [$NaAlCO_3(OH)_2$] were found as irregular inclusions with a vein-like appearance, although their primary or secondary origin was unknown (figure 11C, D). Additionally, magnetite and mica (paragonite and muscovite series) were identified.

Quantitative LA-ICP-MS analysis of trace elements on the 23 samples—90 spots in total—is summarized in table 1 and figure 12. Six of the samples had both blue and yellow bodycolors, and only one had a single yellow bodycolor (again, see figure 10). The other 16 contained numerous inclusions and fractures, and were not clear in color distribution. Chemical analyses were conducted on three spots for each blue, yellow, and included zone. The blue zones had high Fe content ranging 2630 to 3486 ppma and low to medium V content of 0.13 to 0.37 ppma. Their Ti concentration was higher than their Mg content. Ga/Mg ratios for the blue zones varied from 3.50 to 25.35. The yellow zones showed similar Fe, V, and Ga contents as the blue zones, with high Fe (2923 to 3846 ppma), low to medium V (0.13 to 0.40 ppma), and Ga/Mg ratios of 7.78 to 10.06. Included zones also showed similar concentrations of all elements as the blue and yellow zones, although some spots tended to be slightly high in Fe, Ti, Al, and Ga. Enrichment in these elements probably indicates compositions of dense inclusion phases, because most of the inclusion phases were Fe-Ti oxides such as hematite and ilmenite, as documented by Bui et al. (2015) and Narudeesombat et al. (2016). *G&G* previously published that other trace elements, such as Zr, Nb, Ta, W, Th, and U, were enriched in the included zones of some golden sheen sapphires (again, see Winter 2016 Lab Notes, pp. 413-414). Only Ta and U were detected in our samples. Elements such as Na and K that can be considered to be related to inclusions were also detected in some spots on included zones.

TABLE 1. Average and range of trace-element concentration of gold sheen sapphires (in ppma).

Sample	Mg	Ti	V	Cr	Fe	Ga	Ga/Mg ratio
Blue zone (6 samples, 18 spots)	5.88 (1.70–9.29)	13.13 (11.00–19.51)	0.24 (0.13–0.37)	bdl	3258 (2841–3486)	37.67 (31.88–45.04)	10.06 (3.50–25.35)
Yellow zone (7 samples, 21 spots)	8.00 (1.95–15.99)	19.38 (9.26–40.22)	0.26 (0.13–0.40)	bdl	3404 (2923–3846)	39.83 (34.32–46.31)	9.08 (2.65–22.90)
Included zone (17 samples, 51 spots)	8.49 (1.95–23.24)	21.56 (3.63–52.5)	0.10 (bdl–0.56)	bdl	3477 (2630–4552)	39.92 (31.78–53.23)	7.78 (2.29–24.89)

Detection limits: 0.049 for Mg, 0.335 for Ti, 0.035 for V, 0.409 for Cr, 5.28 for Fe, and 0.010 for Ga. bdl: below detection limit.

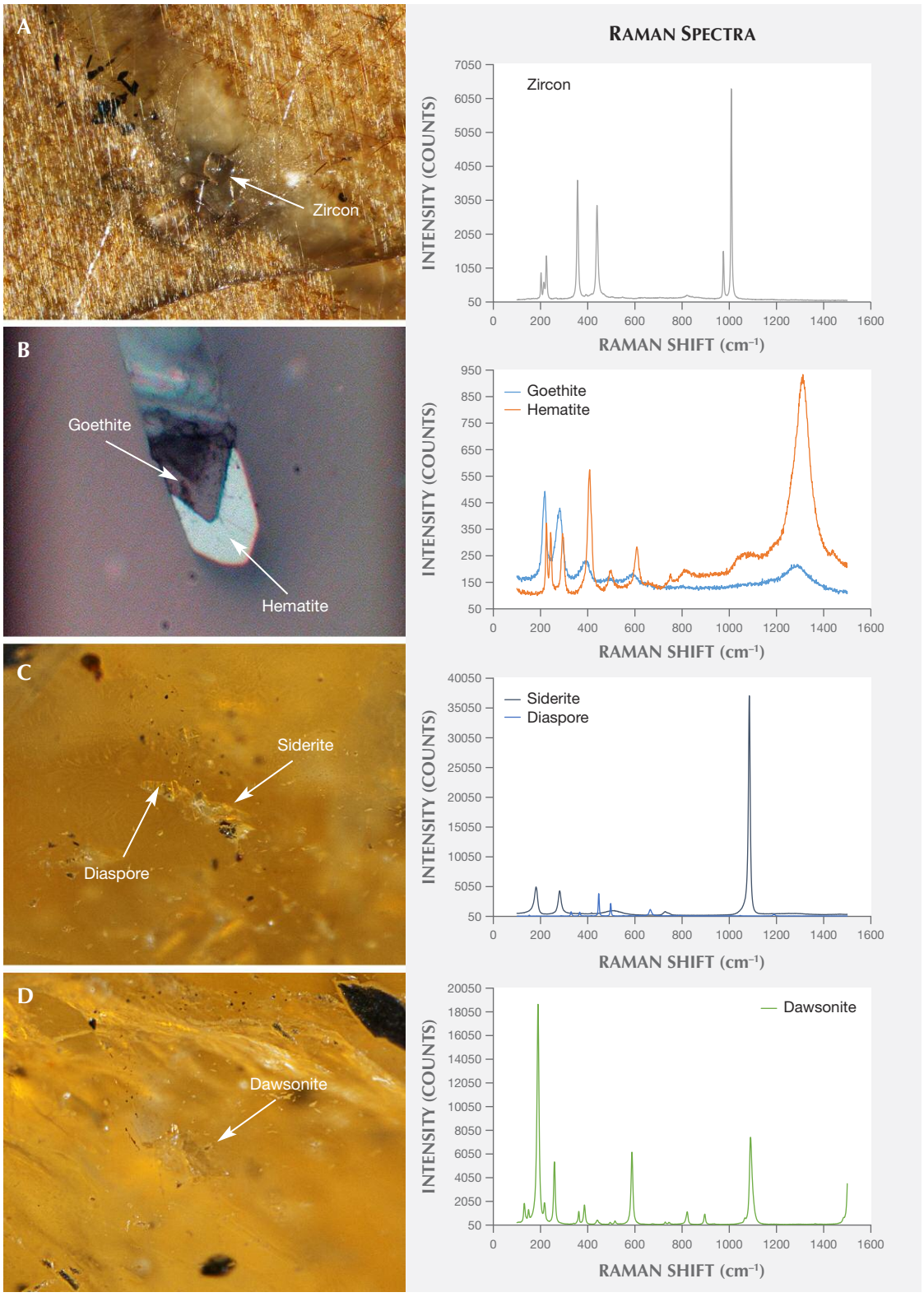

Figure 11. Photomicrographs (left) and Raman spectra (right) of micro-inclusions in golden sheen sapphires: zircon inclusion with intersecting needles (A), hematite and goethite inclusion (B), diaspore and siderite inclusion (C), and dawsonite inclusion (D). Darkfield illumination (A, C, and D) and reflected light (B). Photomicrographs by Makoto Miura; fields of view 1 mm (A), 0.06 mm (B), and 0.8 mm (C and D).

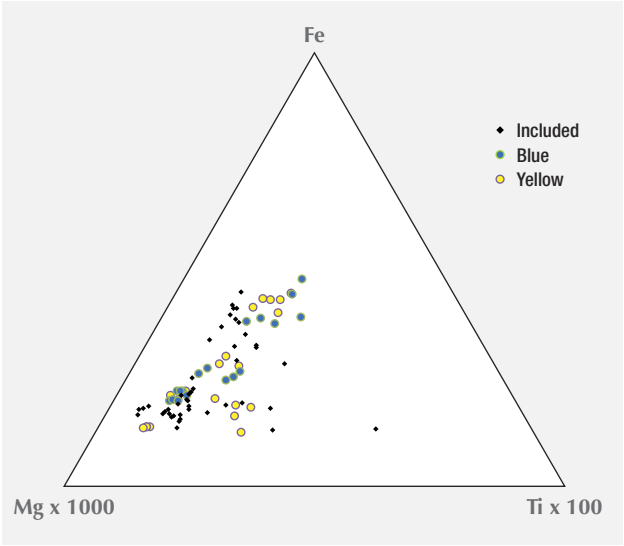

Figure 12. This ternary diagram shows the relationships between Fe, Mg, and Ti in golden sheen sapphires. Note that most of samples have similar Fe, Mg, and Ti content. Some of the yellow and included zones are rich in Mg and Ti.

While golden sheen sapphires are reportedly mined in northeastern Kenya, there is no other published chemical data available from this region. We compared our chemical characteristics with those of other samples documented in the Winter 2016 Lab Notes entry; metamorphic sapphires from Sri Lanka, Myanmar, and Madagascar; and basalt-related sapphires from Thailand, Australia, Nigeria, Kenya, and Cambodia (figure 13). Compositional data for metamorphic and basalt-related sapphires are from previously published articles (J.J. Peucat et al., "Ga/Mg ratio as a new geochemical tool to differentiate magmatic from metamorphic blue sapphires," *Lithos*, Vol. 98, 2007, pp. 262–274; V. Pardieu et al., "Sapphires from the gem rush Bemainty area, Ambatondrazaka (Madagascar)," *GIA News from Research*, Feb. 24, 2017; W. Soonthorntantikul et al., "An in-depth gemological study of blue sapphires from the Baw Mar mine (Mogok, Myanmar)," *GIA News from Research*, Feb. 24, 2017; Fall 2017 GNI, pp. 380–382). As shown in figure 13, the samples in this study were similar to other golden sheen sapphires in Fe, Ga, and V contents. The Fe concentration and high Ga/Mg ratio (table 1) were far from those of metamorphic sapphires but close to those of some basalt-related sapphires. Kenya, where golden sheen sapphires may occur, has two known types of sapphire deposits; one is associated with alkali basalts from the Gregory Rift, an eastern branch of the African Rift Valley, and the other is associated with syenite (Peucat et al., 2007). Both types of sapphire showed a high Fe concentration and Ga/Mg ratio, which are similar to the chemical data in this study.

The similarities in inclusions and trace-element composition between our samples and other golden sheen sapphires indicate that they possibly come from the same origin. A wide variety of inclusions observed in golden sheen sapphires suggests the specific condition during the formation processes. The presence of hematite inclusions especially implied formation in a highly oxidized environment. Further gemological studies are required to construct the database for origin determination.

Makoto Miura, Yusuke Katsurada, and Kazuko Saruwatari
GIA, Tokyo

DIAMONDS

D-color natural IIa diamond with walstromite inclusion. Nondestructive testing methods such as Raman, photoluminescence (PL), and infrared spectroscopy have been

Figure 13. Log plots of chemical variations of Fe vs. Ga contents (expressed in ppma) in golden sheen sapphires. Only blue sapphire data was plotted.

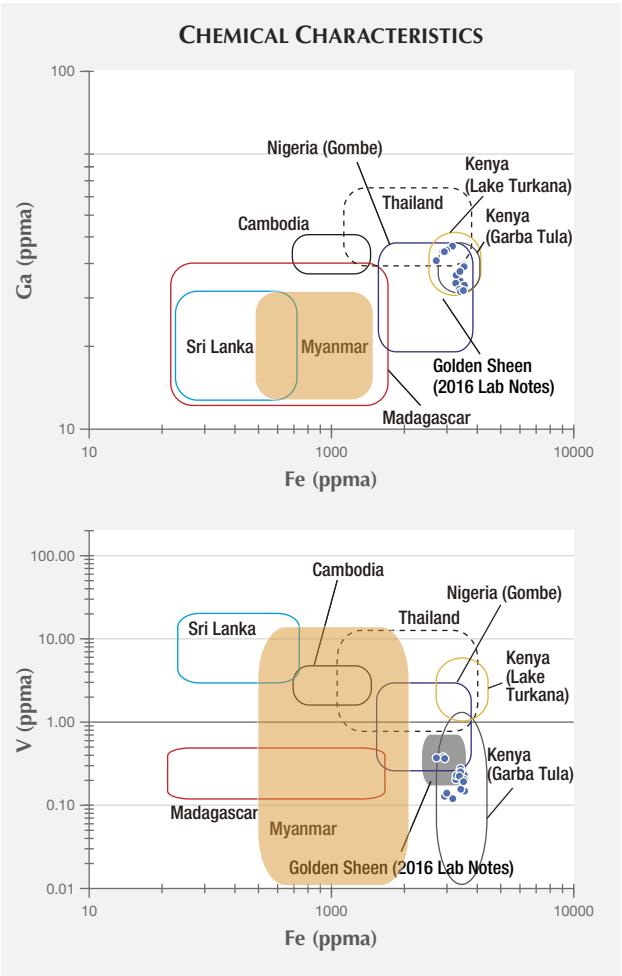

widely applied to identify diamond and its inclusions. The $NV^{0/-}$ (nitrogen-vacancy) and V^0 (vacancy) centers are used as a probe to confirm whether the color of a type IIa diamond is natural or caused by high-pressure, high temperature (HPHT) treatment or irradiation (Fall 2016 Lab Notes, pp. 299–301; D. Fisher et al., "The vacancy as a probe of the strain in type IIa diamonds," *Diamond and Related Materials,* Vol. 15, No. 10, 2006, pp. 1636–1642).

Recently, the National Gemstone Testing Center (NGTC) laboratory in Shenzhen received a 3.0 ct diamond for identification. The stone was a standard round brilliant cut with D color, SI_2 clarity, and a diameter of 9.2 mm. When exposed to DiamondView imaging, the diamond exhibited medium blue fluorescence. It was identified as type IIa because no nitrogen- or boron-related absorptions were detected in the 800–1400 cm^{-1} range and at 2802 cm^{-1}. Nitrogen-vacancy centers NV^0 (575 nm) and NV^- (637 nm) were not detected, either.

Magnification revealed some mineral inclusions and fan-shaped fractures (figure 14). Part of the fissure was filled with black material. We identified the inclusion in figure 14 as $CaSiO_3$-walstromite and confirmed that the black fracture contained graphite using a Renishaw inVia micro-Raman confocal microscope equipped with a green solid laser (532 nm) focused through a 50× short-working-distance objective (figure 15). As the most abundant Ca-bearing mineral inclusion found in super-deep diamonds, $CaSiO_3$-walstromite is believed to derive from $CaSiO_3$-perovskite. Perovskite-structure minerals are predominant in the earth's lower mantle more than 600 km below the surface. The presence of $CaSiO_3$-walstromite and Ca-silicate inclusions is a strong indication of superdeep origin (C. Anzolini et al., "Depth of formation of superdeep diamonds: Raman barometry of $CaSiO_3$-walstromite inclusions," *American Mineralogist*, Vol. 103, No. 1, 2018, pp. 69–74).

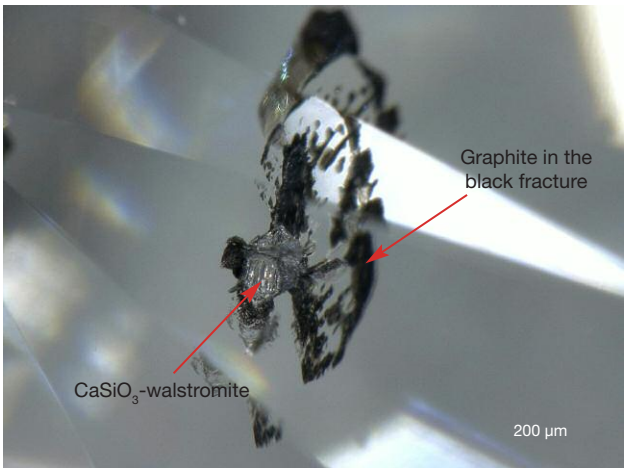

Figure 14. A $CaSiO_3$-walstromite inclusion (100 µm) in a 3.0 ct diamond with fan-shaped black fractures. Graphite (less than 10 µm) was identified in the black fracture. Photomicrograph by Ying Ma.

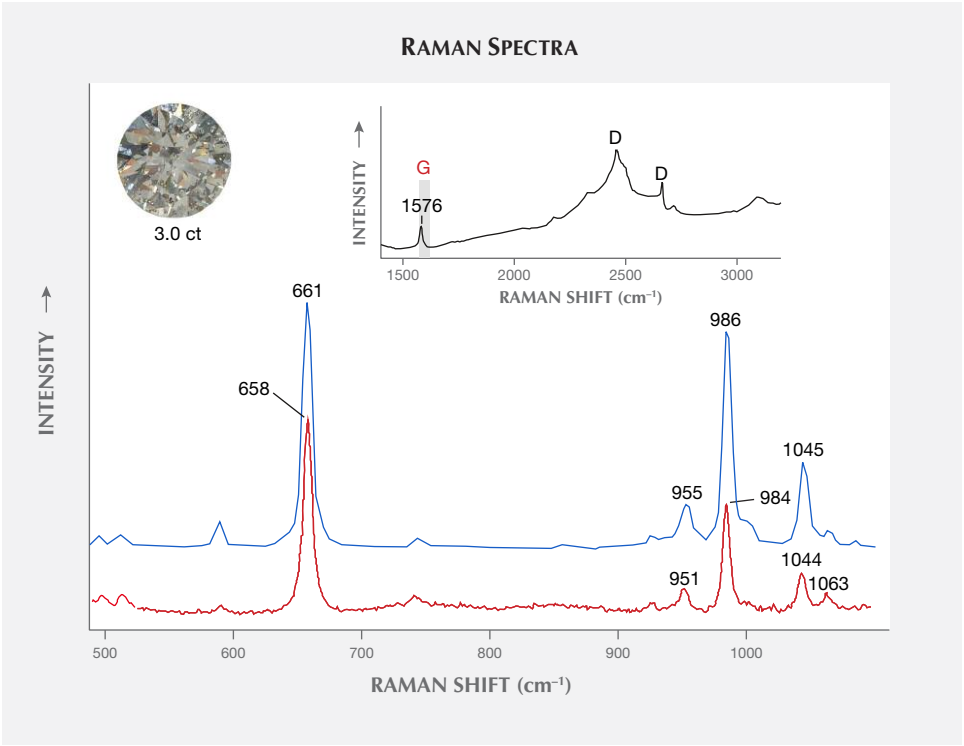

Figure 15. In these Raman spectra, the blue line represents a reference spectrum for $CaSiO_3$-walstromite (Smith et al., 2016, supplementary materials; 500–1100 cm^{-1}). The red trace is from $CaSiO_3$-walstromite in the 3.0 ct diamond (500–1100 cm^{-1}) in the inset photo. The black line shows that the fissure is filled with black graphite; the peak at 1576 cm^{-1} is the G band of graphite, and the D peaks belong to diamond.

Figure 16. In this DiamondView image of the 3.0 ct diamond, the black arrow indicates the site of dislocation networks. Image by Ying Ma.

The 3.0 ct diamond was similar to CLIPPIR (Cullinan-like, Large, Inclusion-Poor, Pure, Irregular, and Resorbed) diamonds (E.M. Smith et al., "Large gem diamonds from metallic liquid in Earth's deep mantle," *Science*, Vol. 354, No. 6318, pp. 1403–1405). Many CLIPPIR diamonds are of top color grades and type IIa, originating from a depth between 360 and 750 km. Dislocation networks, a relatively common feature in type IIa diamonds, were also found (figure 16). Dislocation networks in diamond are interpreted to be equivalent to the polygonized structure of dislocations in other minerals that have been deformed and subsequently annealed (H. Kanda et al., "Change in cathodoluminescence spectra and images of type II high-pressure synthetic diamond produced with high pressure and temperature treatment," *Diamond and Related Materials*, Vol. 14, No. 11-12, 2005, pp. 1928–1931; K. De Corte et al., "Overview of dislocation networks in natural type IIa diamonds," Fall 2006 *G&G*, pp. 122–123). High-temperature experimental treatment of synthetic type II diamond can also reproduce dislocation structures (H. Kanda et al., 2005; D. Fisher et al., "Brown colour in natural diamond and interaction between the brown related and other colour-inducing defects," *Journal of Physics: Condensed Matter*, Vol. 21, No. 36, 2009, 364213).

CLIPPIR diamonds sometimes exhibit infrared absorption at 3107 cm^{-1}; this is a nitrogen-bearing (VN_3H) defect (J.P. Goss et al., "Identification of the structure of the 3107 cm^{-1} H-related defect in diamond," *Journal of Physics: Condensed Matter*, Vol. 26, No. 14, 2014, 145801). This diamond has no clear signature of infrared absorption at 3107 cm^{-1} or NV centers (PL: 575 and 637 nm). We believe that the cause of this is an extremely low level of nitrogen, below the detection limits of the instrument (figures 17 and 18). The lack of nitrogen in type IIa diamond is associated with less color in the diamond. This diamond has a strong V^0-GR1 center (741, 745 nm) and no $NV^{0/-}$(575 nm) and V^0 (637 nm) centers (figure 18).

The $CaSiO_3$-walstromite inclusion in this 3.0 ct diamond indicates a natural diamond from a very deep origin.

Ying Ma, Huihuang Li, Xiaoxia Zhu, Ting Ding, Taijin Lu, and Zhili Qiu
National Gemstone Testing Center (NGTC)
Shenzhen, China

RESPONSIBLE PRACTICES

Gemstones and Sustainable Development Knowledge Hub. In 2016, the Tiffany & Co. Foundation awarded the University of Delaware (UD) $350,000 over the course of two years to promote responsible practices in the colored gemstone

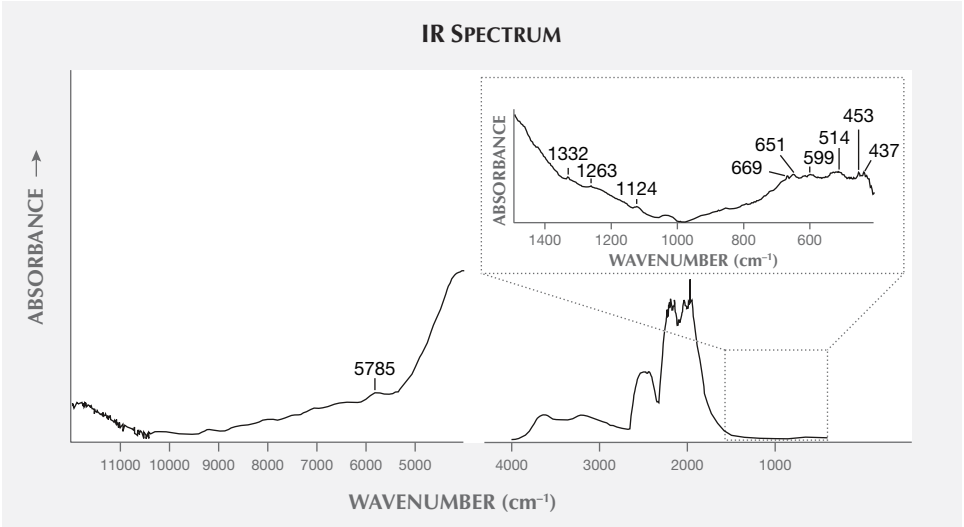

Figure 17. The diamond's infrared spectrum shows no detectable nitrogen-related absorption in the 800–1400 cm^{-1} range. The diamond absorption peak is at 1332 cm^{-1}, while the peaks at 5785, 1263, 1124, and 437–669 cm^{-1} are unknown.

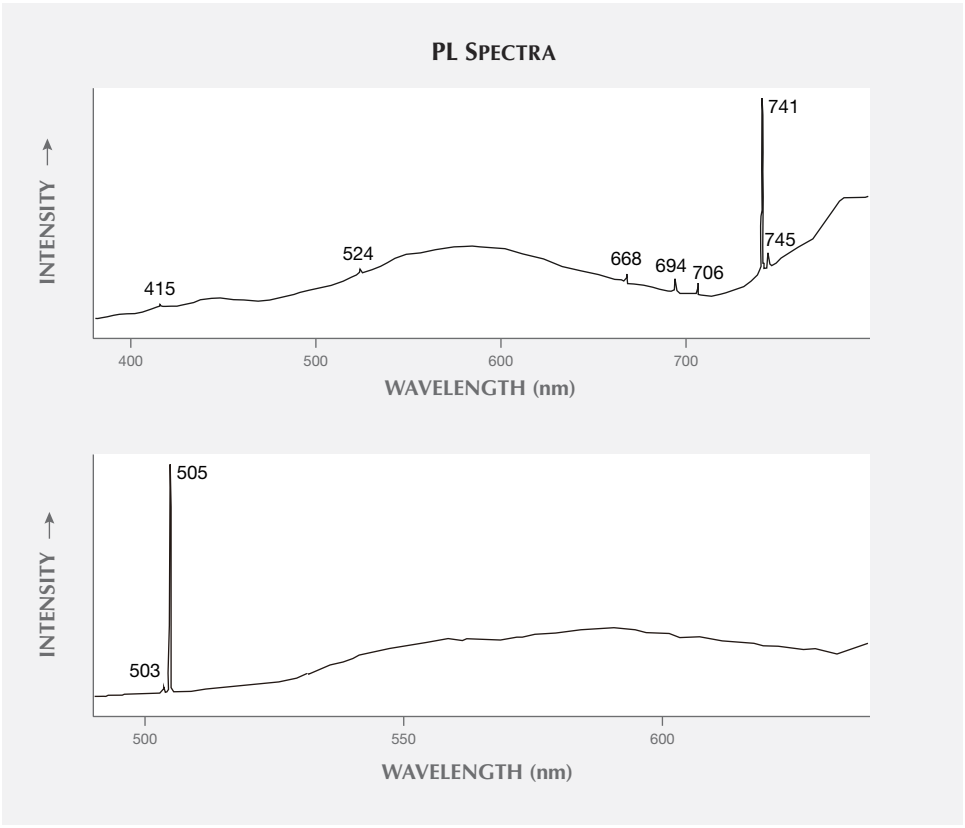

Figure 18. The diamond has a strong V^0-GR1 center (741, 745 nm) and a weak $(NVN)^0$ center (503 nm). The NV^0 (575 nm) and NV^- centers (637 nm) were not detected at liquid nitrogen temperature at either 325 nm (top) or 473 nm (bottom) laser excitation. The designation of the 505, 524, 668, 694, and 706 nm bands is unknown.

supply chain. Out of this grew the Gemstones and Sustainable Development Knowledge Hub, a collaboration between UD, the University of Queensland, and the University of Lausanne. The Hub's goals are to perform research and to connect with initiatives identified by industry, academic, and mining communities as essential to the supply chain. The Hub's website, www.sustainablegemstones.org, is an excellent resource for those interested in learning about and buying sustainable and ethical stones. The areas addressed by the Hub are colored stone mining and geology, processing and manufacturing (including cutting), gender analysis of supply chains, and economic development impact.

Figure 19. Gem cutters in Jaipur were issued masks, provided by AGTA, as part of the safety measures put in place after the Hub's assessment. Photo courtesy of Lynda Lawson.

As of June 2018, the Hub had launched two projects. The pilot project, initiated in Jaipur, India, in early 2018, is a study of the health issues associated with gemstone manufacturing and their solutions. This effort is in partnership with the American Gem Trade Association (AGTA) and Workplace Health Without Borders (WHWB). As part of this program, dust and silica were monitored and cost-effective best practices for improving conditions were evaluated. From these observations, educational materials on silica exposure prevention and other safety precautions, such as the distribution of face masks (figure 19), were created. Noise levels have also been measured, and information on hearing loss, along with disposable hearing protection, has been disseminated. Future steps will involve measuring whether the methods that have been implemented (e.g., wetting to minimize dust and wet mopping of cutting shops) are adequate or if further measures must be taken.

Figure 20. The women miners in Madagascar use the gem testing kit, which includes tweezers, a bowl, a loupe, a dichroscope, and a scoop. Photo courtesy of Lynda Lawson.

The second project is a continuation of the work performed by Lynda Lawson, one of the Hub's research associates, and focuses on miner education in Madagascar. Women miners in the region of Atsimo-Andrefana were taught field gemology essentials and provided with tools for identification (figure 20), even learning to make and use a simple dichroscope. The women were also taught basic lapidary skills, allowing them to make their own jewelry for sale. In the most recent training, the miners have been taught to identify characteristics of stones that are easily confused, such as topaz and quartz; women who had taken previous courses acted as peer coaches. The women have maintained their skills and tools, and the project has been extended through the end of 2018. Future steps will include working with the women to find more profitable markets for the small stones they find (primarily pink, purple, and orange sapphires).

An additional Hub grant was awarded to "Minerals and Society," an interdisciplinary graduate certificate program due to launch at UD in 2020. The program, which will be offered online and on campus, will be designed for members of the jewelry industry along with geologists, economists, and government employees. The program's signature project will be the Jewelry Development Index (JDI), a project first developed at the 2017 Jewelry Industry Summit in Tucson, Arizona. The JDI's goal is to measure the gem and jewelry industry's impact on the economic and social well-being of the countries in which they operate while establishing replicable examples of responsible activity and transparency. UD will begin to develop the JDI in the fall of 2018.

For more information on these programs, please go to www.gia.edu/gems-gemology/summer-2018-gemnews-gemstones-and-sustainable-development-knowledge-hub.

Jennifer-Lynn Archuleta and Aaron Palke
GIA, Carlsbad

Gemstone Guidebook Project. *Selecting Gem Rough: A Guide for Artisanal Miners* was researched, photographed, written, and produced by GIA and distributed in Tanzania through a joint venture between GIA and the nongovernmental organization Pact. It is an educational tool to help artisanal and small-scale miners understand the value of rough gem material. The pilot program was launched in four villages in the Tanga/Umba area of northern Tanzania in the first half of 2017. The sites were selected by Pact staff, who also helped deliver the content and monitor the impact of the training. The region produces a variety of garnets (figure 21), sapphire, tourmaline, and zircon.

Figure 21. A miner in northern Tanzania examines rhodolite rough from a local deposit. Photo by Robert Weldon/GIA.

Figure 22. Gemologist Marvin Wambua (right) shows women miners how to use the white tray to sort gem rough. Photo by Robert Weldon/GIA.

The guidebooks, written in Swahili and showing different types of gem rough found in the area, were distributed to the Tanzanian miners along with small white trays. These trays are used to sort gem rough in reflected or transmitted light (figure 22), which allows stones of higher quality to be separated.

The pilot program reached approximately 200 miners. Participants were surveyed afterward on the effectiveness of the training, and many reported a better understanding of gem quality. Women miners in particular said the training gave them a greater sense of financial independence, indicating that they might be more likely to sell rough on their own rather than rely on men. Using the responses to the survey, Pact calculated that for every $1 invested in the program there was a $12 social return on investment.

In their impact report, GIA and Pact identified areas that might benefit from this resource. GIA has decided to proceed with the project, with plans to include a number of gem localities throughout Tanzania. This expansion is expected to take place in late 2018 and in 2019.

Jennifer-Lynn Archuleta

SYNTHETICS AND SIMULANTS

Observation of etched surface micro-features on HPHT synthetic diamonds using laser confocal microscopy. China is the world's largest HPHT synthetic diamond producer, with an annual output of more than 3,000 tons of rough industrial diamonds. The production technology of HPHT synthetic diamond is quite mature, and most Chinese HPHT synthetic diamonds use the hexahedral static pressure method. The diamond crystals grow out of high-purity graphite through a high-temperature and high-pressure process, and then the superfluous graphite is removed by acid cleaning (Z. Song et al., "Identification characteristics of large near-colourless HPHT synthetic diamond from China," *Journal of Gems and Gemmology*, Vol. 18, No. 3, 2016, pp. 1–8).

Acid cleaning of HPHT synthetic diamond is usually done with 90% H_2SO_4 and 10% HNO_3. This process can remove graphite and metal impurities that remain on the diamond surface and in crevices (L. Yin et al., "Micromechanism of the artificial diamond's growth," *Journal of Synthetic Crystals*, Vol. 29, No. 4, 2000, pp. 386–387). During the growth process, the metal catalyst and graphite are in close contact with diamond and continuously participate in crystal growth.

To the best of our knowledge, no research has been done on the surface characteristics of HPHT synthetic diamonds after acid cleaning, which can reveal the growth features of HPHT diamond. In this study, 39 HPHT synthetic diamonds produced in China were observed using laser confocal microscopy (LCM). The laser confocal microscopy measures the surface topography of the sample moving focused laser spots over the sample with a galvanometer scanner. The strongest-intensity scanning points in each vertical scan layer are recorded and used to construct the 3-D topography through a pixel-by-pixel method (W.-C. Liu et al., "A self-designed laser scanning differential confocal microscopy with a novel vertical scan algorithm for fast image scanning," *IFAC-PapersOnLine*, 2017, Vol. 50, No. 1, 2017, pp. 3221–3226). Therefore, the laser confocal microscope can overcome the problem of depth of field and observe the surface characteristics of materials clearly.

The characteristics of the structure after acid cleaning are observed on the surface of an HPHT synthetic diamond and on the inside of the crystal. An HPHT synthetic diamond was cut into thin slices and then washed by acid, exposing its internal structure (figure 23). Metal catalysts and a small amount of graphite remain in diamond crystals

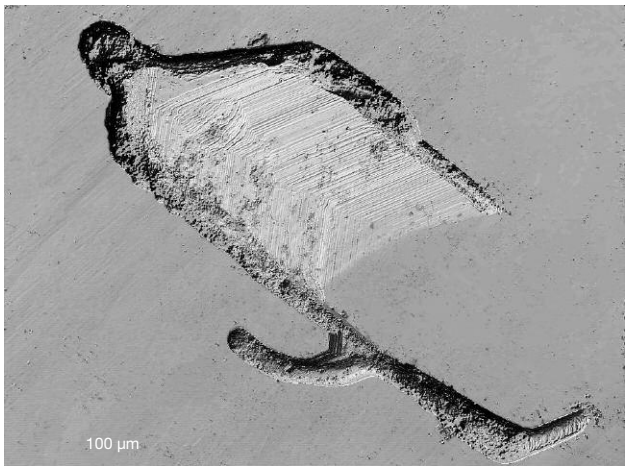

Figure 23. Laser confocal microscopy (LCM) shows traces of metallic catalyst and step-like growth marks in an HPHT synthetic diamond's interior. Photo by Xuxu Wu.

during growth, leaving holes in the interior. Due to the lack of raw material for growth in the hole, a step-like structure was left in the space that was not fully filled with crystallized diamond.

The fine structure of the step-like growth can be expressed by using the 3D scanning function of the laser confocal microscope. The images built in the three-dimensional coordinate system can show the depth and spatial relationship of the microstructures (figure 24). The irregularly etched structures, the depth of voids left by metal catalysts, range from 5 to 17 µm.

After acid cleaning, HPHT synthetic diamonds will display step-like irregular pits and lines on the surface (figure 25). The triangular growth structures of HPHT synthetic

Figure 24. 3D scanning of micro-features by LCM shows the depth change and relative spatial relation. Image by Xuxu Wu.

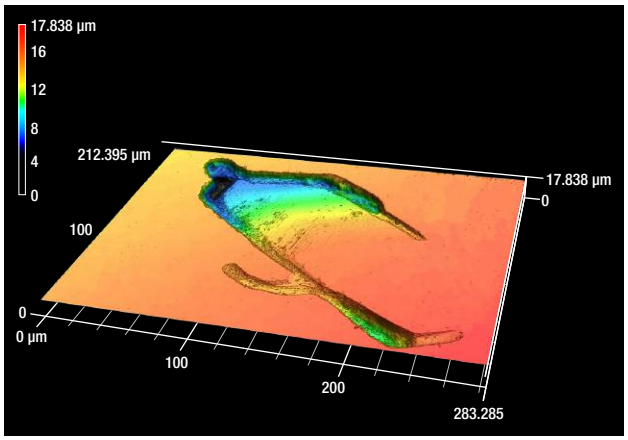

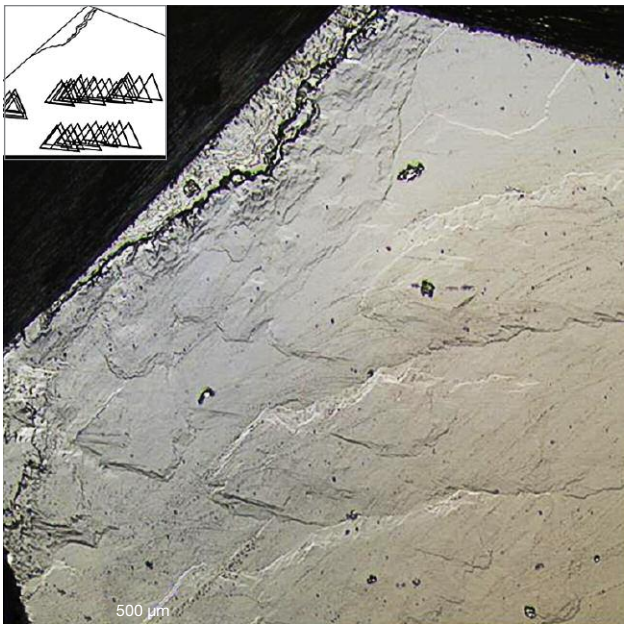

Figure 25. Step-like irregular pits and lines on the surface of the HPHT synthetic diamond. The inset shows a simulation of the sample's stacked triangular growth structure. Photo by Xuxu Wu.

diamonds are stacked on the surface with slight displacement. Rectilinear line marks on the surface of HPHT synthetic diamonds (figure 26) are also very common, and may be traces of the displacements that develop between small

Figure 26. The surface of this HPHT synthetic diamond presents several groups of parallel lines. Photo by Xuxu Wu.

Figure 27. Two white jade bracelets weighing 62.305 g (left) and 69.422 g (right) with dark color patches similar to the natural skin of some nephrite pebbles. Photo by Jianjun Li.

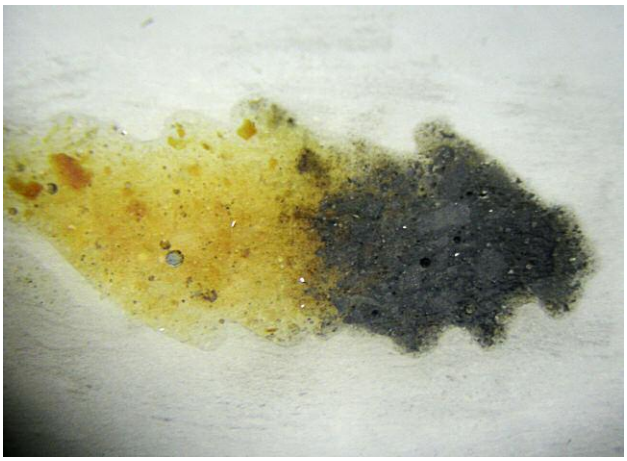

Figure 28. Many gas bubbles and spherical pores formed from burst bubbles can be seen in the brown and black areas. Photo by Jianjun Li; field of view 13 mm.

crystals due to compression during the growth process.

Characteristic patterns observed on the surface of HPHT synthetic diamonds are related to metal catalysts and diamond particles, revealing the order of growth of synthetic diamonds. The step-like structure with the same angle is very common. The etched microstructure caused by metal catalysts usually displays irregular patterns. The several groups of parallel straight lines could be caused by the displacement and friction between a large number of tiny diamonds in the growth chamber. LCM is very reliable at revealing surface micro-features on HPHT synthetic diamonds, and it should be more widely applied to gemological research.

Contributors' note: This study was partially supported by the National Natural Science Foundation of China (grants 41473030 and 41272086).

Xuxu Wu, Taijin Lu, Shi Tang, Jian Zhang, Zhonghua Song, Hua Chen, and Jie Ke
NGTC, Beijing
Mingyue He
China University of Geosciences, Beijing

TREATMENTS

Nephrite bracelet with filled cavity. Nephrite, also called tremolite, is treasured by the Chinese for its fine texture and superior toughness. White nephrite pebbles with some areas of orange or brown skin are called *zi yu*. Mutton-fat nephrite jade with a natural dark brown, brown, and/or brown-yellow oxide skin is rare and considered premium quality. This skin forms due to natural weathering, and the pebble is polished within river currents. In China, nephrite enthusiasts often aspire to own mutton-fat *zi yu* jewelry. White jade that is artificially polished into pebbles and partially dyed is often seen in China as an imitation of mutton-fat jade with brown and/or orange skin. Therefore, many traders treat the white primary ore into dyed brown-orange pebbles by artificially dyeing the material. A great deal of white jade with partially dyed color is marketed as mutton-fat *zi yu* in the Chinese market.

Recently, China's National Gold & Diamond Testing Center (NGDTC) laboratory received from a client two bracelets with filled cavities that mimicked mutton-fat nephrite with dark brown skin. This treatment process is quite different from the traditional surface staining.

Shown in figure 27 are two bracelets weighing 62.305 and 69.422 g. The white portions were pure with very fine texture. The deep brown parts, which resembled the black skin on some nephrite, were distributed along large fissures, and the sharp color boundaries were accompanied by brown and yellow materials. The black material penetrated the body of the 62.305 g bracelet (figure 28).

Standard gemological tests were carried out to identify the two bracelets and the deep brown and orange-yellow parts. With the owner's permission, a dark brown portion was sampled with a knife to obtain small scrapings, which were mixed with KBr powder to form a tablet. Next, infrared spectra were collected using a Nicolet Nexus 470 infrared spectrometer with a resolution of 8 cm^{-1} and 64 scans per sample.

With a PIKE Technologies UpIR diffuse reflection accessory, reflectance infrared spectra were collected on the white parts of the bracelets. The instrument resolution and scan count were the same as those described above. The reflection spectrum was corrected using the Kramers-Kronig method.

The sample's spot RI was 1.61; the SG ranged between 2.95 and 2.96, consistent with nephrite. The white body of the bracelets presented very weak blue-white fluorescence under a 5-watt long-wave UV lamp (365 nm) and was inert under short-wave UV (254 nm). Because of a poor surface

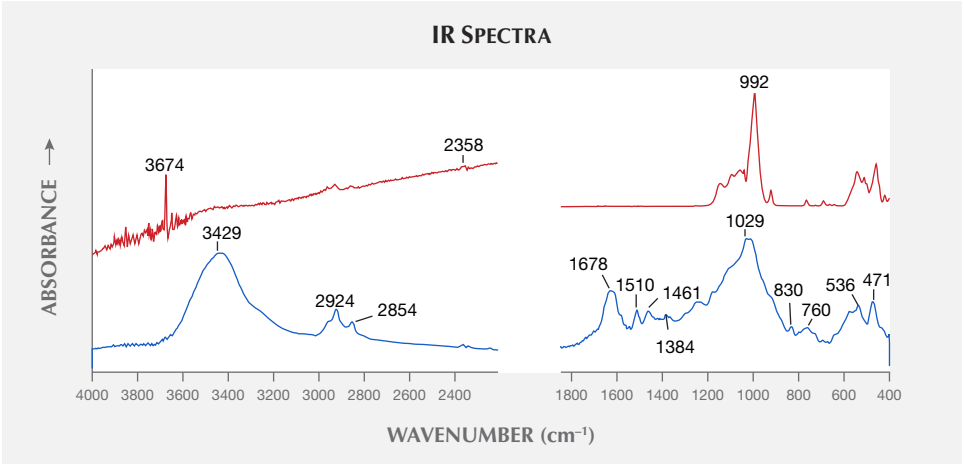

Figure 29. Infrared spectra of the white (red line) and brown (blue line) areas of the bracelets are significantly different, with fingerprints that represent the vibration of the -OH (3674 cm^{-1}) and the -CH_2- groups (2924 and 2854 cm^{-1} peaks), respectively. The spectra have been vertically offset for clarity.

polish, the refractive index of the brown-black part could not be measured. The dark parts showed no fluorescence.

Under the gemological microscope, the white bodies presented a cryptocrystalline texture, with some obscure white areas. Dark brown patches on the bracelets appeared compact, with a slightly weak luster and grainy texture. The dark patches on the inner wall of one bracelet contained many spherical pores and gas bubbles of different sizes (again, see figure 28). This feature is common in glass or plastic imitation gemstones, but has never been found in nephrite. Spherical pores are formed from bubbles close to the surface that burst during the polishing process. The brown or dark brown dendritic pattern often found in fractures of natural nephrite (Z. Yin et al., "Nephrite jade from Guangxi Province, China," Fall 2014 *G&G*, pp. 228–235) was not observed. Magnification showed that the orange-yellow and dark brown patches were artificially filled.

One of the authors reported on a "filled nephrite" in 2005 (J. Li, "The identification of impregnated nephrite," *Australian Gemmologist*, Vol. 22, No. 7, pp. 310–317). After careful testing, a serious mistake in that report has subsequently been identified: the direct transmission FTIR spectra with absorption bands or peaks between 3060 and 2850 cm^{-1} were incorrectly attributed to the epoxy resin filler. The nephrite in that report was not actually filled at all. Until now, the authors have not found a nephrite that has been bleached and filled with polymer like the B-jadeite jade. The author of the earlier study and a coauthor of the present study (JL) no longer believe that direct transmission infrared spectroscopy detects the treatment of nephrite jade. The author tried to collect direct transmission infrared spectra through the deep brown patches of the two bangles, but experiments show that these areas absorbed the mid-infrared light completely.

As shown in figure 29, there was significant difference between the infrared spectra of the white body (collected using reflection mode) and the brown patches (collected with KBr powder). These clearly represent two different materials.

The infrared spectrum (red line in figure 29, right) from the white body of the bracelets has a fingerprint similar to that of Italian nephrite (see I. Adamo and R. Bocchio, "Nephrite jade from Val Malenco, Italy: Review and update," Summer 2013 *G&G*, pp. 98–106), except that the sample does not exhibit the absorption peak of carbonate-associated minerals. This verifies that the white part of the sample is tremolite.

To identify the material in the dark brown part collected with KBr powder (blue line in figure 29, right), we searched databases containing hundreds of spectra libraries purchased by NGDTC using Thermo Scientific OMNIC 9.2 software. Materials with higher degrees of matching included allspice, cellophane, and even opium. This suggests that the dark brown material may be organic. Further advanced testing would be required to conclusively identify the dark brown material.

In the 4000–2000 cm^{-1} range, the white part shows a spectrum peak of 3674 cm^{-1}, attributed to the stretching vibration of the -OH groups in tremolite; the dark brown part shows a strong absorption band centered at 3429 cm^{-1} between 3700 and 3100 cm^{-1}. This band is usually associated with hydroxyl groups in the polymer in organic matter. The 2924 and 2854 cm^{-1} peaks are often attributed to the -CH_2- groups, which often appear in the spectra of organic-filled gems (e.g., E. Fritsch et al., "Identification of bleached and polymer-impregnated jadeite," Fall 1992 *G&G*, pp. 176–187; M.L. Johnson et al., "On the identification of various emerald filling substances," Summer 1999 *G&G*, pp. 82–107). Contamination from human fingerprints or body oils can also lead to absorption peaks within the 3000–2800 cm^{-1} range, but the absorption is generally weaker. The spectrum of the white part of the sample has a very weak absorption in this region, probably due to human body fat contamination or wax residue left after polishing.

This evidence indicates that the dark brown and orange parts of the samples are fillers. But this filling is obviously different from that in B-jade, where polymer is flooded between the grain boundaries. The filling in these two nephrite bracelets looks more like that in single-crystal gems. Therefore, we propose that the nephrite used in these bracelets had severe pits or cavities, and fillers were

used to fill them and make the surface look smooth. The authors want to alert the trade and consumers to this new treatment, whose detection requires access to gemological instruments. Therefore, bringing your nephrite jewelry to a gem laboratory can help avoid unnecessary loss.

Jianjun Li and Guihua Li
National Gold & Diamond Testing Center
Shandong Province, China

Haixia Chen
Gemstone and Materials Technology Institute
Hebei Geoscience University, China

Separating glass-filled rubies using the DiamondView. The treatment of gemstones using various filler materials is not new. In the case of corundum, silica glass was often observed filling rubies from approximately 1980 to the early 2000s, when it was largely replaced by high-lead-content glass in early 2004 (S.F. McClure et al., "Identification and durability of lead glass–filled rubies," Spring 2006 *G&G*, pp. 22–34) which has since become the mainstream artificial filler in corundum. The Lai Tai-An Gem Lab in Taipei recently examined a pair of rubies (figure 30) that were quickly determined to be glass filled with the assistance of DiamondView imaging. In our experience, the DiamondView detects the presence of glass, although it does not distinguish between different types of glasses. This note shows how the DiamondView can be used to observe the presence and, perhaps more importantly, the degree of filling in rubies.

The two heart-shaped cabochons weighed 6.81 and 6.89 ct and measured approximately 10.78 × 13.55 × 5.39 mm and 11.36 × 13.10 × 5.47 mm, respectively. Each semitransparent stone exhibited a purplish red color and fluoresced a strong red to long-wave ultraviolet radiation while exhibiting a weak red reaction to short-wave ultraviolet irradiation. Standard gemological testing showed spot RIs of 1.76, and SGs of 3.94 and 3.93, respectively, which were lower than regular values and raised suspicion that the stones were filled, while advanced analysis by energy-dispersive X-ray fluorescence (EDXRF) and FTIR spectroscopy and Raman microscopy revealed data consistent with ruby. Magnification with a gemological microscope revealed natural fluid and fingerprint inclusions, but some evidence of a filler was also observed in the fractures.

Figure 30. A pair of rubies that were determined to be glass filled, partly with the assistance of DiamondView imaging. Photo by Lai Tai-An Gem Lab.

Under the DiamondView's visible light settings, some surface-reaching filler features and filled "cavities" were also revealed. Notable differences in the surface reflectance between the filling material and surrounding corundum (figure 31) were clearly evident. After exposure to the DiamondView's short-wave UV radiation, the treated nature of both rubies was even more apparent as the reaction not only showed the obvious cavities but the extent of the filler (in blue) running throughout the stones (figure 32). The 6.81 ct ruby revealed an even greater degree of filling than its twin, especially on the base where a greater concentration of filling material was noted.

As the DiamondView results prove, filler materials penetrate or remain on the fractures of the treated material (ruby in this case) under certain treatment conditions. Hence, some filling treatments may be revealed more clearly when exposed to the ultra-short-wave energy of the DiamondView. Chemical analysis of a filled area using EDXRF detected Si and Ba as the major elements. Minute

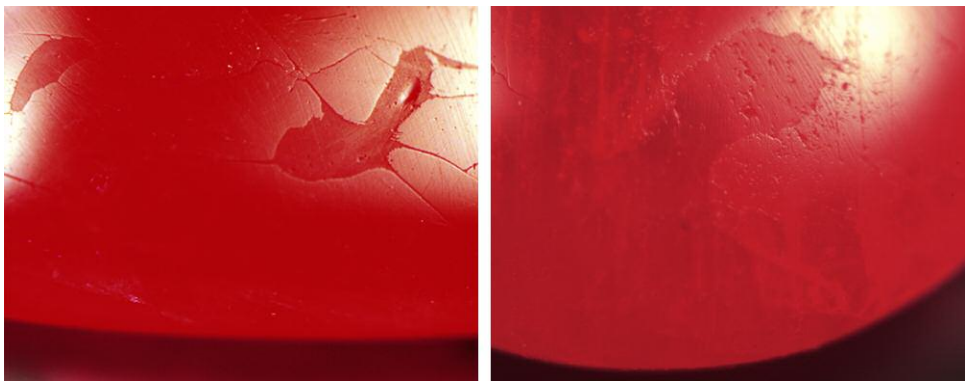

Figure 31. Notable differences in the reflectance of the glass filling and corundum host were seen in the DiamondView's visible light mode.

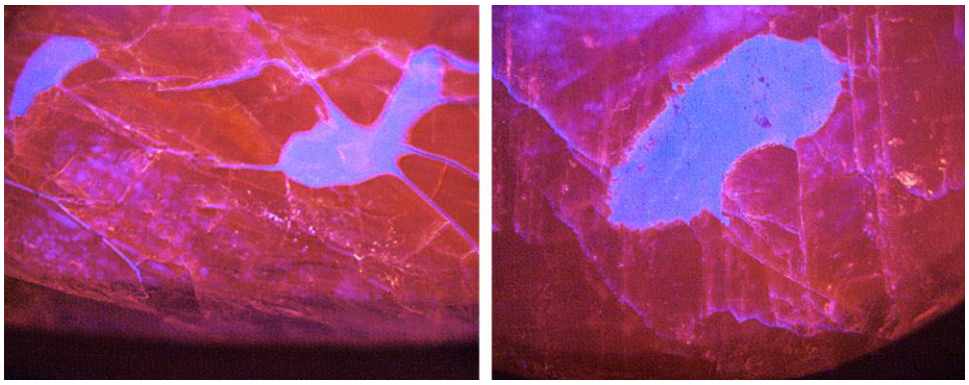

Figure 32. In contrast to figure 31, the DiamondView's operational mode clearly revealed the glass-filled cavities as well as the extent of the glass (shown in blue) running throughout the rubies.

levels of Pb were also obtained. The results proved the filler was a glass composed of these elements, which were not detected when other filler-free areas were analyzed.

Artificial glass is frequently used as a filling material in gemstones. The variable chemical compositions of these different glasses help improve the appearance (lower visibility of fractures) of the host after treatment. While the vast majority of glasses and other fillers, both organic and inorganic, can be detected with a loupe or microscope, the DiamondView is a useful identification aid should the need arise.

Larry Tai-An Lai (service@laitaian.com.tw)
Lai Tai-An Gem Laboratory, Taipei

Strong fluorescence in B-jade impregnated with wax. Fine-quality jadeite jade is known for its high value in the market. "A," "B," and "C" jade are classifications applied to jadeite that relate to various states of enhancement. However, many in the market may not understand the real meaning of the terms. A-jade shows no indications of having undergone modification through the impregnation with colorless or near-colorless wax, resin, or any other agent. When the material has been treated through bleaching and the impregnation with colorless or near-colorless wax, resin, or any other agent, it is described as B-jade. When it shows indications of having fissures or fractures filled with a color agent, it is defined as C-jade. B and C areas may exist in the same specimen; this is described as B+C-jade. A bangle submitted to the Lai Tai-An Gem Laboratory (figure 33, left) illustrates the common misconception that B jade is only impregnated by resin. In fact, wax-impregnated jadeite jade is also defined as B-jade.

The client who submitted the bangle believed it was resin-impregnated jadeite owing to its suspiciously strong fluorescence reaction. The item possessed an uneven green and white color with a greasy luster and weighed 277.14 ct. It measured approximately 76 mm with a thickness of 9–10 mm. An RI reading of 1.66 was obtained from five

Figure 33. Left: The wax-impregnated jadeite jade bangle submitted for identification. Right: The bangle exhibited strong bluish fluorescence under long-wave UV radiation. Photos by Lai Tai-An Gem Lab.

Figure 34. Microscopic observation revealed obvious acid etching marks, coarse pits, and cobweb-like surface fissures. Photo by Lai Tai-An Gem Lab; field of view 4.6 mm.

random spots on the bangle, and an SG of 3.34 was also recorded. The most interesting feature was an unusually strong reaction under long-wave UV (figure 33, right), indicating it was probably treated and should be examined with more care. This material was determined to be jadeite jade when subsequently tested by FTIR spectroscopy, but the FTIR results also revealed some features other than the jadeite-related peaks.

FTIR analysis confirmed that the jadeite bangle was heavily impregnated with wax. The absorption peaks at 2850, 2920, and 2965 cm^{-1} differed from those expected in resin-impregnated material—which usually exhibits peaks at 3061 and 3040 cm^{-1}—and they were intense and sharp enough to indicate that a significant quantity of wax had been applied. Microscopic examination revealed obvious acid etching marks, coarse pits, and cobweb-like surface fissures (figure 34). Wax residues were also found within pits and fissures when poked. Additional unseen wax was apparently within the structure according to the wax pattern revealed by FTIR analysis, typical for wax-impregnated B-type jadeite, which clearly explains the strong reaction under long-wave UV.

While the term B-jade is meant to be applied to wax- and/or resin-impregnated material (Laboratory Manual Harmonisation Committee Information Sheet #11, http://www.lmhc-gemology.org/pdfs/IS11_20111215.pdf), many traders misleadingly describe B-type jadeite jade as resin-impregnated only. This leads the unsuspecting buyer to believe that wax-impregnated jadeite jade is A-jade. This case clearly shows that those dealing in jadeite should be aware of the differences between resin- and wax-impregnated materials, even though both are considered B-jade, and understand that confusion may arise if items are not carefully checked.

Larry Tai-An Lai

CONFERENCE REPORTS

IAC conference on responsible gold. Gold: Vortex, Virtues, and Values was hosted by Initiatives in Art and Culture (IAC) at Bohemian National Hall in New York City, April 12–13. Now in its eighth year, the conference has become an annual industry gathering for those looking to evaluate the market, discover exceptional work, and discuss key gold-related issues.

Mark Hanna (Richline Group) opened the conference, stating that it is the leading gold event in the United States and introducing IAC founder **Lisa Koenigsberg**, who discussed the importance of bringing together people from various backgrounds. "Gold is the substance that can rivet our attention because the reality is the thing we ascribe value to in a social compact. Everyone in this room agrees that this has value."

In the kickoff presentation, **Jeffrey Christian** (CPM Group) presented graphs showing that interest rates and gold prices are not correlated but indicated that surplus labor will become a problem due to computer-assisted manufacturing. Christian recommended gold as a way to diversify investment portfolios. In assessing international gold investment demand, he concluded that Indian gold investment is in long-term decline and that Chinese gold investment, while down from 2013, is ultimately rising.

Next was the update from Washington, DC. **Tiffany Stevens** (Jewelers Vigilance Committee) addressed the status of Federal Trade Commission (FTC) guides, which are meant to champion consumers and protect them from unfair competition. Once the guides are issued, the JVC will translate them for the industry. Highlighting hot topics, Stevens addressed service applications of precious metals, advertising and disclosure, and anti-money laundering efforts. **Susan Thea Posnock** (Jewelers of America) discussed the importance of advocacy, touching upon hearings on sales tax fairness that could reflect the changing marketplace. **Elizabeth Orlando** (U.S. Department of State) discussed her team's work with conflict minerals and diamonds, particularly regarding the Kimberley Process and the Dodd-Frank Act. **Mark Hanna** observed that the requirement for new FTC members to review regulations has slowed down the overall process. **Linus Drogs** (AU Enterprises) addressed regulations that dictate what can and cannot be marked "Made in the USA" domestically versus globally.

Andrea Hill (Hill Management Group) reframed the use of technology in business. Hill emphasized the importance of marketing coherently across platforms and offering customers help with the decision-making process. She noted that consumers generally shop online and buy in-store. Making the experience seamless over the phone and approaching marketing from the standpoint of consumer desire are key.

Next, **Brandee Dallow** (Fine Girl Luxury Brand Building & Communications) had a sit-down with jewelry designer **Alexandra Mor**, who is working with Balinese artisans to

promote the tagua nut as a luxury alternative to elephant ivory. Taking innovation to the next level, Mor has created a material out of tagua that can be 3D printed to solve the problem of the nut's limiting size.

Independent consultant **Christina Miller** moderated a session on sustainable jewelry. Miller laid out international commitments regarding responsible sourcing, celebrating the progress made and hoping "to push the needle further" during the gold conference. **Monica Stephenson** (idazzle.com and Anza Gems) spoke on the importance of reinvesting in source communities. **Wing Yau** (WWAKE) discussed sourcing in Colombia, where she has visited model mines. **Blair Lauren Brown** (VERTE Essentials) talked about the 120-year legacy of the Alaskan gold nugget jewelry she works in and how it supports local mining. **Stewart Grice** (Hoover & Strong) noted that the company imports from Peru, Colombia, and Mongolia, bringing gold to the U.S. and either selling it as 24K or karating the materials for use. The premium on fair-mined products goes back directly to the local communities. Third-generation retailer **Robert Goodman** (Robert Goodman Jewelers) discussed his commitment to bringing in designers dedicated to sustainability. **Nina Farran** (Fashionkind) came to the table with a style slant. Fashionkind, which stands for "fashion in humankind," began as a blog before launching a retail platform. The group also spoke of industry collectives driving down prices in sustainable sourcing as consumer education drives the demand for sustainable products.

After the sustainability panel, **Toby Pomeroy** was presented with IAC's inaugural award for Leadership and Responsible Practice in Jewelry. The award recognizes a transformational contribution to the worldwide gem and jewelry industry. A leader in the responsible sourcing movement, Pomeroy also founded the Mercury Free Mining Challenge, which seeks to discover a safe replacement for mercury.

Next, **Jean-Jacques Grimaud** (SolidWorks Sell) delivered a presentation on optimizing the consumer experience through personalization. Technology keeps the customer fully engaged with the product, while brands are able to maintain control of design integrity. Grimaud demonstrated a sample personalized software for ring design that is accessible from a computer, tablet, or phone—all on the cloud.

Thursday's closing panel on blockchain technology was jointly presented by **Mark Hanna**, **Marla Beck Hedworth** (UL), and **Catherine Malkova** (IBM). The overview of blockchain technology included provenance assured by the blockchain ledger, permissions to ensure visibility and security, consensus by all parties to verify transactions, immutability, smart contracts, and finality once an operation is completed. Trustchain is proposed to be a consortium permissioned private blockchain, focused on the provenance of a diamond engagement ring from the diamond and gold mines, tracking the full supply chain from the mine to the end consumer.

In the evening, IAC hosted "A Rising Tide: Women in the Jewelry Industry." **Hedda Schupak** (Centurion) moderated the discussion, and panelists included: designer **Wendy Brandes**, **Brandee Dallow**, **Jenny Luker** (Platinum Guild International), and **Barbara Palumbo** (Adornmentality.com and WhatsOnHerWrist.com). A variety of topics were addressed, including: women's involvement in political movements and willingness to perform unpaid labor to promote change, the increase of more women working independently due to lack of upward mobility in corporate settings, minimal presence of women on industry boards for products directing marketing towards women, and more.

Day two started with "Moda Operandi: A New Business Model for Jewelry." **Mickey Alam Khan** (Mobile Marketer) interviewed **Deborah Nicodemus** (Moda Operandi). The company's online luxury business model is currently based on three channels: trunk shows, boutique business, and the showroom. Of the three models, only the boutique carries inventory.

A panel moderated by **Rob Bates** (JCK) that included **David Bouffard**, **Toby Pomeroy**, **Christina Miller**, **Tiffany Stevens**, and **Elizabeth Orlando** opened by discussing issues related to gold. Orlando detailed the smuggling of artisanally mined gold, money laundering problems, gold's use to support armed groups and cartels, and labor problems such as the U.S. interest in eliminating forced labor, mercury use, deforestation, and wildlife trafficking. Bouffard spoke on Signet's efforts to identify the sources of its gold. After years of coordination and tracking from banks to refineries, Signet now knows where 99% of its gold comes from. The company is on the ground to make sure gold that comes from the legitimate supply chain and that workers are paid fair wages, helping promote a responsible cycle. Stevens described how the JVC office helps the industry combat money laundering. Pomeroy noted that his group is raising a million-dollar prize for a safe alternative to mercury in gold mining. Miller spoke about the Initiative for Responsible Mining Assurance and its work on large-scale mining standards. Five sectors form the current setup: mining companies, purchasing companies, labor unions, NGOs, and mining-affected communities. She concluded by reminding the audience that we rely on mining every day, so as an industry we need to advocate for it to be done responsibly.

Leo and Ginnie de Vroomen, the husband-and-wife designers behind the de Vroomen brand, presented selections from their stunning body of work, including the step-by-step making of a gold repoussé bangle. They use brightly colored gemstones and enamel and a variety of traditional metalsmithing techniques to create sculptural forms.

Enameler **Jane Short** detailed her more than 40 years of enameling. Her enamel is focused on the interplay of color or self-expression. Short presented examples of enamel throughout history, explaining technique and chronicling the creation of an enamel on silver beaker.

Figure 35. Barbara Palumbo, Monica Stephenson, and Sarah Yood participate in the panel "Who's Got the Power? Influencers, Ethics, and the Regulations of Social Media." Photo by Alice Catherine Young.

Next, designer **Jen Townsend**, **Renée Zettle-Sterling** (Society of North American Goldsmiths), and **Lin Stanionis** (University of Kansas) spoke on casting. Townsend and Zettle-Sterling are co-authors of the new book *CAST: Art and Objects Made Using Humanity's Most Transformational Process*, which covers jewelry, architecture, and everyday objects made by casting. They described how life events influenced their designs and later inspired them to write the book to combat the stigma associated with the process. The pages feature exceptional cast work, from ancient jewelry to computer-aided design. Stanionis related how casting is a part of her jewelry design process. She explained her dedication to expressing human experience. Her pieces use organic forms such as rattlesnake vertebrae, bones, cracked eggshells, and leaves. She and her husband also excavate fossils and incorporate elements such as dinosaur bones, memorializing links to the past.

Andrea Hill returned to moderate "Industrial Revolution 4.0: Cultivating and Perpetuating Old World Skills." **Patricia Madeja** (Pratt Institute) noted that our country must do more to appreciate makers. **Ted Doudak** (RIVA Precision Manufacturing) added that there are rules for supply and demand—we should see where the demand is, understand what crafts need to be filled, and encourage those. He also emphasized the importance of valuing artisans by compensating them well and acknowledging their accomplishments. **Rich Youmans** (MJSA), **Katrin Zimmermann** (Ex Ovo), and designer goldsmith **Ann Cahoon** rallied around education and the importance of teaching and apprenticeships outside the family.

"Who's Got the Power? Influencers, Ethics, and the Regulations of Social Media" ended the conference with a follow-up panel from last year. **Sarah Yood** (Jewelers Vigilance Committee), **Barbara Palumbo**, **Wendy Brandes**, and **Monica Stephenson** (figure 35) interacted with the audience, under the moderation of **Peggy Jo Donahue**. Yood explained that the FTC is monitoring social media channels, and action can be taken if material connections between influencers and products are not clearly disclosed. She urged the audience to review the FTC endorsement guides and a new Frequently Asked Questions section on their website regarding the endorsement guides. Other topics included early disclosure of sponsorship on posts, pitching, and the purchasing of fake followers. Stephenson added, "Generosity, plus vulnerability, plus accountability, plus candor, equals trust." The panel also took up the issue of followers, and how the question of how many followers an influencer had was usually brought up before getting to know the influencer. The use of fake and purchased followers has also become rampant.

The excitement around the annual IAC conference was palpable. Attendees anticipated a spectrum of calls to action after the gathering. The networking opportunities and the chance to appreciate gold among like-minded colleagues made for an enjoyable and enlightening experience. To learn more about the conference and other upcoming IAC events, visit www.artinitiatives.com.

Olga González
New York